Future Circular Collider

Precision physics programme

Precision Physics at the FCC-ee

Hamzeh Khanpour

hamzeh.khanpour@agh.edu.pl

Faculty of Physics and Applied Computer Science

AGH University of Krakow

Seminarium HEP Bialasowka

15 May 2026

Contents

Part I

Precision Physics at the FCC-ee

Chapter 1

Physics Background and Precision Physics at the FCC-ee

1.1 FCC-ee as a precision machine

The Future Circular Collider programme is designed as an integrated precision-plus-energy-frontier strategy. The electron–positron stage, FCC-ee, would operate at several centre-of-mass energies chosen to maximise sensitivity to different sectors of the Standard Model: the Z pole, the WW threshold, the ZH Higgs stage, the $t\bar{t}$ threshold and a high-energy 365 GeV stage. The hadron stage, FCC-hh, then uses the same infrastructure to extend direct reach and high-energy precision. The relevant point for this talk is that rare top searches at FCC-ee are not disconnected from the rest of the programme: they exploit the same clean event reconstruction, vertexing, flavour tagging and global interpretation logic that define the Higgs and electroweak programmes [1, 3, 2].

Definition

A precision observable is an experimentally measurable quantity whose Standard-Model prediction and experimental uncertainty can be controlled well enough that small deviations become meaningful. Examples include m_Z, Γ_Z, $\sin^2\theta^\ell_{\text{eff}}$, $\sigma(ZH)$, m_W, m_t and rare branching fractions such as $\text{Br}(t \to q\gamma)$.

In an effective-field-theory picture, the sensitivity of a precision observable to heavy new physics can be estimated schematically as

$$\frac{\delta\mathcal{O}}{\mathcal{O}_{\text{SM}}} \sim C_i \frac{v^2}{\Lambda^2}, \tag{1.1}$$

for observables controlled by electroweak symmetry breaking, or as

$$\frac{\delta\mathcal{O}}{\mathcal{O}_{\text{SM}}} \sim C_i \frac{E^2}{\Lambda^2}, \tag{1.2}$$

for high-energy amplitudes whose deviations grow with the scattering energy E. Here C_i is a dimensionless Wilson coefficient, $v \simeq 246\,\text{GeV}$ is the Higgs vacuum expectation value and Λ is the characteristic new-physics scale. A per-mille measurement therefore probes multi-TeV scales for order-one Wilson coefficients. This simple estimate is only a guide; real interpretations require correlations, theory uncertainties, detector effects and EFT validity checks.

Key message

The first scientific message of the talk is that precision measurements and rare processes are complementary discovery tools. Precision Higgs, electroweak and top measurements test correlated deviations, while top-FCNC searches test interactions that are essentially absent in the SM.

Table 1.1: Assumed running scenarios for representative future-collider options. The entries summarise the initial state, geometry, beam polarisation assumptions, centre-of-mass energies and integrated luminosities used for comparison studies.

Collider	**Initial state**	**Geometry, # IPs**	**Beam polarisation**	$\sqrt{s}$	$\mathcal{L}_{\text{int}}$
LEP3	e^+e^-	Circular, 2 IPs	Unpolarised	91.2 GeV	48 ab^{-1}
				160 GeV	5.6 ab^{-1}
				230 GeV	2.304 ab^{-1}
FCC-ee	e^+e^-	Circular, 4 IPs	Unpolarised	91.2 GeV	205 ab^{-1}
				161 GeV	19.2 ab^{-1}
				240 GeV	10.8 ab^{-1}
				365 GeV	3.12 ab^{-1}
LCF	e^+e^-	Linear, 1 IP	$(\mp 80\%, \pm 30\%)$	91.2 GeV	0.1 ab^{-1}
				250 GeV	3 ab^{-1}
				350 GeV	0.2 ab^{-1}
				550 GeV	4 (8) ab^{-1}
			$(\mp 80\%, \pm 20\%)$	1000 GeV	8 (0) ab^{-1}
FCC-hh$^{(*)}$	pp	Circular, 4 IP	Unpolarised	84 TeV	30 ab^{-1}
MuCol3$^{(*)}$	$\mu^+\mu^-$	Circular, 2 IP	Unpolarised	3 TeV	1 ab^{-1}
MuCol10$^{(*)}$	$\mu^+\mu^-$	Circular, 2 IP	Unpolarised	10 TeV	10 ab^{-1}
LHeC$^{(*)}$	e^-p	Hybrid, 1 IP	Unpolarised	1.2 TeV	1 ab^{-1}

Notes: IP denotes interaction point. The starred entries are included as broader future-collider comparison scenarios. The FCC-ee luminosities correspond to the four-IP baseline comparison assumptions shown in the source table. For the linear-collider option, the two luminosities shown in parentheses denote alternative running assumptions at the corresponding energy.

1.2 Why Z, WW, Higgs and top measurements are correlated

The FCC-ee programme is best understood as a network of measurements. The Z pole fixes electroweak vertices and pseudo-observables. The WW threshold tests the charged-current gauge sector and the W mass. The Higgs stage measures $\sigma(ZH)$ inclusively and exclusive Higgs decay rates. The top threshold and 365 GeV stage constrain m_t, Γ_t and top electroweak couplings. In the Standard Model Effective Field Theory (SMEFT), the same gauge-invariant operators can contribute to several of these sectors simultaneously:

$$\mathcal{L}_{\text{SMEFT}} = \mathcal{L}_{\text{SM}} + \sum_i \frac{C_i^{(6)}}{\Lambda^2}\mathcal{O}_i^{(6)} + \sum_i \frac{C_i^{(8)}}{\Lambda^4}\mathcal{O}_i^{(8)} + \cdots . \tag{1.3}$$

A single-operator interpretation of one Higgs rate is usually too naive, because electroweak data may constrain the same direction. Conversely, Higgs rates can help interpret electroweak and top deviations. This is the reason for Slide 13: Higgs precision needs the Z and WW programmes.

1.3 Electroweak pseudo-observables and $Zf\bar{f}$ couplings

At the Z pole, the collider scans the resonance line shape and measures partial widths and asymmetries. The most important pseudo-observables include

$$m_Z, \quad \Gamma_Z, \quad \sigma^0_{\text{had}}, \quad R_\ell, \quad R_b, \quad R_c, \quad A^{0,f}_{\text{FB}}, \quad \sin^2\theta^\ell_{\text{eff}}, \quad N_\nu. \tag{1.4}$$

The hadronic pole cross section is

$$\sigma^0_{\text{had}} = \frac{12\pi}{m_Z^2}\frac{\Gamma_e\Gamma_{\text{had}}}{\Gamma_Z^2}. \tag{1.5}$$

The ratios

$$R_\ell = \frac{\Gamma_{\text{had}}}{\Gamma_{\ell\ell}}, \qquad R_b = \frac{\Gamma_{b\bar{b}}}{\Gamma_{\text{had}}}, \qquad R_c = \frac{\Gamma_{c\bar{c}}}{\Gamma_{\text{had}}} \tag{1.6}$$

remove some common systematics and isolate flavour-dependent electroweak couplings. The effective number of light neutrinos can be expressed schematically as

$$N_\nu = \frac{\Gamma_{\text{inv}}}{\Gamma_\nu^{\text{SM}}}, \tag{1.7}$$

where Γ_{inv} is the invisible Z width after subtracting the visible partial widths. Deviations in N_ν may arise from new invisible particles or modified neutrino couplings, but precision interpretation requires careful control of the full Z-width fit.

1.3.1 Chiral couplings

The Z boson couples differently to left- and right-handed fermions. Define the chirality projectors

$$P_L = \frac{1-\gamma_5}{2}, \qquad P_R = \frac{1+\gamma_5}{2}, \qquad f_L = P_L f, \quad f_R = P_R f. \tag{1.8}$$

A useful convention is

$$\mathcal{L}_{Zff} = \frac{g}{c_W} Z_\mu \bar{f}\gamma^\mu \left(g_L^f P_L + g_R^f P_R\right) f, \tag{1.9}$$

with

$$g_L^f = T_3^f - Q_f \sin^2\theta_{\text{eff}}^f, \qquad g_R^f = -Q_f \sin^2\theta_{\text{eff}}^f. \tag{1.10}$$

Right-handed SM fermions are singlets under $SU(2)_L$, so $T_3 = 0$ for their weak isospin. Left-handed fermions sit in $SU(2)_L$ doublets and have $T_3 = \pm 1/2$. The vector and axial combinations are conventionally related by

$$g_V^f = g_L^f + g_R^f, \qquad g_A^f = g_L^f - g_R^f, \tag{1.11}$$

up to global normalisation conventions. Partial widths and asymmetries probe different combinations:

$$\Gamma_f \propto (g_L^f)^2 + (g_R^f)^2, \qquad A_f = \frac{(g_L^f)^2 - (g_R^f)^2}{(g_L^f)^2 + (g_R^f)^2}, \tag{1.12}$$

$$A_{\text{FB}}^{0,f} = \frac{3}{4}A_e A_f. \tag{1.13}$$

This is why rates, line-shape information and asymmetries together separate left- and right-handed shifts.

1.4 WW threshold, gauge structure and aTGCs

Near the WW threshold the cross section $e^+e^- \to W^+W^-$ is very sensitive to m_W and Γ_W. Above threshold, differential angular distributions are sensitive to the non-Abelian electroweak gauge structure. A common anomalous triple-gauge-coupling parameterisation is

$$\begin{aligned} \mathcal{L}_{WWV} = &-ig_{WWV}\Big[g_1^V\left(W^+_{\mu\nu}W^{-\mu}V^\nu - W^-_{\mu\nu}W^{+\mu}V^\nu\right) + \kappa_V W^+_\mu W^-_\nu V^{\mu\nu} && (1.14)\\ &+ \frac{\lambda_V}{m_W^2}W^+_{\mu\nu}W^{-\nu\rho}V_\rho{}^\mu\Big], \qquad V = \gamma, Z. && (1.15) \end{aligned}$$

At tree level in the SM,

$$g_1^\gamma = g_1^Z = \kappa_\gamma = \kappa_Z = 1, \qquad \lambda_\gamma = \lambda_Z = 0. \tag{1.16}$$

One needs to consider the $\delta g_{1,Z}$, $\delta\kappa_\gamma$ and λ_Z as the key deviations. Here $\delta g_{1,Z}$ modifies the overall WWZ structure, $\delta\kappa_\gamma$ acts like an anomalous magnetic-dipole contribution to $WW\gamma$, and λ_Z is a momentum-dependent higher-derivative interaction. In SMEFT, these parameters are correlated with Higgs-gauge interactions such as HZZ and HWW.

1.5 Higgs recoil method and absolute coupling extraction

At $\sqrt{s} \simeq 240\,\text{GeV}$, the process

$$e^+e^- \to ZH \tag{1.17}$$

operates near the Higgsstrahlung cross-section maximum. If the Z boson is reconstructed, for example through $Z \to \mu^+\mu^-$ or $Z \to e^+e^-$, the recoil mass is

$$\begin{aligned} m^2_{\text{recoil}} &= (p_{e^+} + p_{e^-} - p_Z)^2 && (1.18)\\ &= s + m_Z^2 - 2\sqrt{s}E_Z, && (1.19)\end{aligned}$$

where E_Z is the reconstructed Z-boson energy. The key point is that this observable does not require reconstructing the Higgs decay. Therefore invisible, exotic or untagged Higgs decays still contribute to the inclusive ZH peak. The inclusive cross section scales as

$$\sigma(ZH) \propto g^2_{HZZ} \equiv \kappa_Z^2 (g^{\text{SM}}_{HZZ})^2. \tag{1.20}$$

This gives the absolute Higgs normalisation that is missing at hadron colliders.

Exclusive Higgs decays then measure products of production and decay factors:

$$\sigma(ZH)\,\text{Br}(H \to X) \propto \frac{g^2_{HZZ} g^2_{HXX}}{\Gamma_H}, \tag{1.21}$$

while WW-fusion gives

$$\sigma(\nu\bar{\nu}H)\,\text{Br}(H \to X) \propto \frac{g^2_{HWW} g^2_{HXX}}{\Gamma_H}. \tag{1.22}$$

Combining recoil, exclusive decays and vector-boson fusion gives direct access to absolute couplings and the total width Γ_H.

1.5.1 Exclusive Higgs decay channels

Mode	Coupling information	Physics role
$H \to b\bar{b}$	bottom Yukawa κ_b	Dominant Higgs decay; central for absolute coupling fits and flavour-tagging performance.
$H \to c\bar{c}$	charm Yukawa κ_c	Direct second-generation quark coupling; requires charm tagging and control of $b/c/g$ separation.
$H \to gg$	effective Hgg modifier κ_g	Loop-induced in the SM; sensitive to top loops, QCD and possible coloured BSM states.
$H \to \tau^+\tau^-$	tau Yukawa κ_τ	Tests third-generation lepton mass generation and tau reconstruction.
$H \to WW^*$	HWW coupling κ_W	Important width handle; one W is off shell for a 125 GeV Higgs.
$H \to ZZ^*$	HZZ coupling κ_Z	Clean gauge-coupling channel and width handle.

$H \to \gamma\gamma$	effective $H\gamma\gamma$ modifier κ_γ	Rare loop-induced mode; FCC-hh statistics strongly improve precision.
$H \to Z\gamma$	effective $HZ\gamma$ modifier $\kappa_{Z\gamma}$	Rare loop-induced mode with strong BSM sensitivity.
$H \to \mu^+\mu^-$	muon Yukawa κ_μ	Second-generation lepton Yukawa; benefits strongly from FCC-hh.

1.6 Higgs coupling modifiers and the κ-3 framework

In the coupling-modifier framework,

$$\kappa_i = \frac{g_i}{g_i^{\rm SM}}, \tag{1.23}$$

for tree-level couplings, while loop-induced processes are assigned effective modifiers such as κ_g, κ_γ and $\kappa_{Z\gamma}$. A production-times-decay rate can be written as

$$(\sigma \cdot {\rm Br})(i \to H \to f) = \sigma_i \frac{\Gamma_f}{\Gamma_H}. \tag{1.24}$$

In the κ framework,

$$(\sigma \cdot {\rm Br})(i \to H \to f) = \left(\sigma_i^{\rm SM}\kappa_i^2\right) \frac{\Gamma_f^{\rm SM}\kappa_f^2}{\Gamma_H^{\rm SM}\kappa_H^2}, \tag{1.25}$$

so that the signal strength is

$$\mu_i^f = \frac{(\sigma \cdot {\rm Br})}{(\sigma \cdot {\rm Br})_{\rm SM}} = \frac{\kappa_i^2\kappa_f^2}{\kappa_H^2}. \tag{1.26}$$

The total-width modifier is approximated by

$$\kappa_H^2 = \sum_j \kappa_j^2 {\rm Br}_j^{\rm SM}, \tag{1.27}$$

with the sum over all relevant SM decay modes. If invisible or untagged modes are allowed, the κ-3 framework often uses

$$\bar{\kappa}_H^2 = \frac{\kappa_H^2}{1 - B_{\rm inv} - B_{\rm und}}, \qquad \Gamma_H = \bar{\kappa}_H^2 \Gamma_H^{\rm SM}. \tag{1.28}$$

The condition $\kappa_V \leq 1$ is sometimes imposed in hadron-collider fits to stabilise the width interpretation. At FCC-ee, inclusive ZH recoil strongly reduces this degeneracy by directly measuring $\sigma(ZH)$.

Caution

The κ framework is useful for explaining Higgs-rate measurements, but it is not a gauge-invariant EFT. SMEFT is required when one wants to connect Higgs, electroweak, diboson and top observables consistently.

1.7 SMEFT interpretation of Higgs, EW and top data

The SMEFT operators most relevant include bosonic operators and current operators. Examples are

$$\mathcal{O}_{HWB} = H^\dagger \sigma^a H W^a_{\mu\nu} B^{\mu\nu}, \tag{1.29}$$

$$\mathcal{O}_{HD} = \left| H^\dagger D_\mu H \right|^2, \tag{1.30}$$

$$\mathcal{O}_{H\ell}^{(1)} = (H^\dagger i \overleftrightarrow{D}_\mu H)(\bar{\ell}\gamma^\mu \ell), \tag{1.31}$$

$$\mathcal{O}_{H\ell}^{(3)} = (H^\dagger i \overleftrightarrow{D}^a_\mu H)(\bar{\ell}\sigma^a\gamma^\mu \ell), \tag{1.32}$$

$$\mathcal{O}_{He} = (H^\dagger i \overleftrightarrow{D}_\mu H)(\bar{e}\gamma^\mu e). \tag{1.33}$$

These can shift Zee couplings, affect HZZ and $HZee$ contact interactions and correlate with diboson and Higgs production. Bosonic operators such as $\mathcal{O}_{HW}$, $\mathcal{O}_{HB}$ and $\mathcal{O}_{W}$ affect gauge-boson kinetic/momentum structures and anomalous triple-gauge couplings. This is the origin of the chords in the circos plot: the plot visualises correlations among fitted effective couplings, not independent measurements (See Fig. 1.1).

1.8 Global Higgs–electroweak interpretation

It is also useful to make explicit why the Higgs programme at FCC-ee cannot be interpreted as an isolated set of Higgs rate measurements. The same electroweak gauge structure that determines Z-pole observables and W^+W^- production also controls the $e^+e^- \to ZH$, $e^+e^- \to \nu\bar{\nu}H$, and diboson amplitudes. Therefore, precision Higgs measurements, electroweak pseudo-observables and triple-gauge-coupling measurements must be combined in a common fit.

In an effective-field-theory language, this statement follows from gauge invariance. The Standard Model Effective Field Theory (SMEFT) expands the low-energy Lagrangian as

$$\mathcal{L}_{\text{SMEFT}} = \mathcal{L}_{\text{SM}} + \sum_i \frac{C_i^{(6)}}{\Lambda^2}\mathcal{O}_i^{(6)} + \sum_i \frac{C_i^{(8)}}{\Lambda^4}\mathcal{O}_i^{(8)} + \cdots , \tag{1.34}$$

where $C_i^{(d)}$ are Wilson coefficients and Λ is the characteristic scale of the heavy new dynamics. A single dimension-six operator can shift several apparently different interactions at once. For example, operators modifying the Zee coupling also affect the extraction of the HZZ coupling in $e^+e^- \to ZH$, and bosonic operators that affect HZZ or HWW interactions can also contribute to anomalous triple-gauge couplings in $e^+e^- \to W^+W^-$.

Definition

Global Higgs–electroweak interpretation. A global interpretation is a fit in which Higgs rates, electroweak pseudo-observables, diboson observables and, where relevant, top observables are fitted simultaneously. The purpose is to account for correlations induced by gauge invariance, common systematic/theory inputs and shared SMEFT operators. In such a fit, the extracted quantity is not just an isolated "Higgs coupling", but a correlated set of effective couplings or Wilson coefficients.

1.8.1 Correlation structure of the FCC-ee Higgs and electroweak fit

Figure 1.1 illustrates the correlation structure among the fitted effective couplings in a global FCC-ee Higgs/electroweak analysis. The plot is a *circos-style* correlation diagram. The labels around the circle denote effective couplings or coupling shifts. The bars outside the circle indicate the projected sensitivity to each coupling, while the chords inside the circle indicate correlations between fitted quantities. A thick chord represents a stronger correlation. The figure should be read in three layers.

First, the outer labels denote effective couplings. These include Higgs couplings, electroweak fermion couplings and anomalous gauge couplings. A typical notation is

$$\delta g^H_{ZZ}, \quad \delta g^H_{WW}, \quad \delta g^H_{\gamma\gamma}, \quad \delta g^H_{Z\gamma},$$

for effective Higgs interactions with electroweak gauge bosons, together with fermionic $Zf\bar{f}$ couplings such as

$$\delta g_L^{Ze}, \quad \delta g_R^{Ze}, \quad \delta g_L^{Z\mu}, \quad \delta g_R^{Z\mu}, \quad \delta g_L^{Zb}, \quad \delta g_R^{Zb},$$

and anomalous triple-gauge couplings such as

$$\delta g_{1,Z}, \qquad \delta\kappa_\gamma, \qquad \lambda_Z.$$

The precise label convention depends on the basis used in the global fit, but the physics message is basis independent: Higgs, electroweak and diboson couplings are correlated.

Second, the bars show the expected precision with different collider inputs. The grey reference bars correspond to the HL-LHC baseline, while the FCC-ee-enhanced bars show the improvement from adding precision FCC-ee measurements. The comparison highlights the role of the Z-pole programme: without very precise $Zf\bar{f}$ information, the Higgs-coupling fit remains partly limited by uncertainties in electroweak vertices.

Third, the chords show correlations. A chord between two couplings means that the fit cannot determine them independently: a shift in one can be partly compensated by a shift in another. The important message is not the existence of one particular chord, but the global pattern. FCC-ee Z-pole and WW-threshold data remove or reduce several degeneracies that would otherwise weaken Higgs-coupling extraction.

Key message

The Higgs programme needs the Z and WW programmes because the same gauge-invariant SMEFT operators modify $Zf\bar{f}$, HZZ, HWW, $HZee$, WWZ and $WW\gamma$ interactions. Precision Z-pole and diboson measurements therefore turn FCC-ee Higgs measurements into a well-constrained global electroweak fit, rather than a set of isolated rate measurements.

1.8.2 Left- and right-handed electroweak couplings

A central class of quantities appearing in Fig. 1.1 is the set of left- and right-handed $Zf\bar{f}$ couplings. These are important because the Z boson couples differently to left- and right-handed fermions. The chirality projectors are

$$P_L = \frac{1-\gamma_5}{2}, \qquad P_R = \frac{1+\gamma_5}{2}. \tag{1.35}$$

The interaction of the Z boson with a fermion f can be written as

$$\mathcal{L}_{Zff} = \frac{g}{c_W} Z_\mu \, \bar{f}\gamma^\mu \left(g_L^f P_L + g_R^f P_R\right) f, \tag{1.36}$$

where g is the weak $SU(2)_L$ coupling and $c_W = \cos\theta_W$. In a common normalisation,

$$g_L^f = T_3^f - Q_f \sin^2\theta_{\text{eff}}^f, \qquad g_R^f = -Q_f \sin^2\theta_{\text{eff}}^f. \tag{1.37}$$

Here T_3^f is the weak isospin of the left-handed fermion and Q_f is its electric charge. Right-handed Standard-Model fermions are $SU(2)_L$ singlets, so they have $T_3 = 0$; left-handed fermions belong to $SU(2)_L$ doublets and have $T_3 = \pm 1/2$.

It is also common to use vector and axial-vector couplings,

$$g_V^f = g_L^f + g_R^f, \qquad g_A^f = g_L^f - g_R^f, \tag{1.38}$$

up to convention-dependent overall normalisations. The partial width and the asymmetry parameter probe different combinations:

$$\Gamma_f \propto (g_L^f)^2 + (g_R^f)^2, \tag{1.39}$$

whereas

$$A_f = \frac{(g_L^f)^2 - (g_R^f)^2}{(g_L^f)^2 + (g_R^f)^2}. \tag{1.40}$$

At the Z pole, the forward–backward asymmetry is approximately

$$A_{\text{FB}}^{0,f} = \frac{3}{4} A_e A_f. \tag{1.41}$$

Thus, line-shape measurements constrain the sum of squared chiral couplings, while asymmetries constrain their relative difference. Combining rates, asymmetries and, where available, polarisation information gives separate sensitivity to g_L^f and g_R^f.

Caution

The notation for effective couplings is convention dependent. In a global fit, symbols such as $\delta g^{Zf}_{L,R}$ denote deviations from the Standard-Model values in a specified normalisation. One should not compare numerical values of δg between papers unless the coupling convention and input-parameter scheme are the same.

1.8.3 Gauge-invariant origin of the correlations

The common origin of the correlations in the circos plot can be understood from representative dimension-six SMEFT operators. For example,

$$\mathcal{O}_{HWB} = H^\dagger \sigma^a H \, W^a_{\mu\nu} B^{\mu\nu}, \tag{1.42}$$

$$\mathcal{O}_{HD} = \left| H^\dagger D_\mu H \right|^2, \tag{1.43}$$

$$\mathcal{O}^{(1)}_{H\ell} = \left(H^\dagger i \overleftrightarrow{D}_\mu H \right) \left(\bar{\ell} \gamma^\mu \ell \right), \tag{1.44}$$

$$\mathcal{O}^{(3)}_{H\ell} = \left(H^\dagger i \overleftrightarrow{D}^a_\mu H \right) \left(\bar{\ell} \sigma^a \gamma^\mu \ell \right), \tag{1.45}$$

$$\mathcal{O}_{He} = \left(H^\dagger i \overleftrightarrow{D}_\mu H \right) \left(\bar{e} \gamma^\mu e \right). \tag{1.46}$$

The operators $\mathcal{O}^{(1)}_{H\ell}$, $\mathcal{O}^{(3)}_{H\ell}$ and $\mathcal{O}_{He}$ shift the Z-boson couplings to leptons after electroweak symmetry breaking. Since the initial state in $e^+e^- \to ZH$ is an electron–positron pair, such shifts also affect the interpretation of Higgsstrahlung. Bosonic operators such as

$$\mathcal{O}_{HW}, \qquad \mathcal{O}_{HB}, \qquad \mathcal{O}_{W} \tag{1.47}$$

modify gauge-boson kinetic structures, momentum-dependent HVV couplings and anomalous triple-gauge couplings. Therefore, Z-pole, WW, Higgs and diboson measurements are not separate theoretical problems: they are different projections of the same gauge-invariant EFT parameter space.

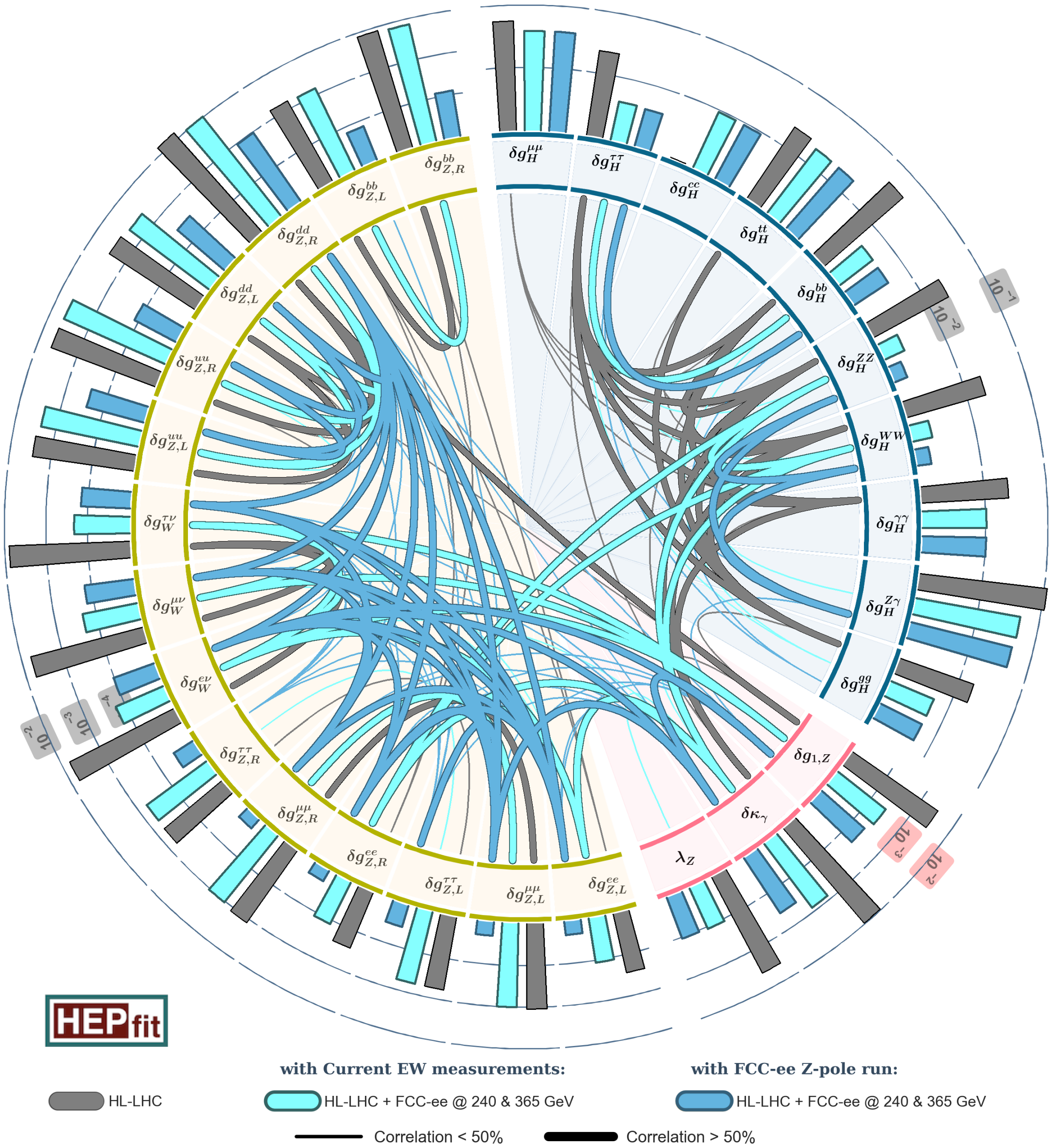

Figure 1.1: Correlation structure in a global FCC-ee Higgs/electroweak fit. The outer bars show the projected sensitivity to effective couplings, while the inner chords show correlations among fitted quantities. The comparison between fits with current electroweak inputs and fits including the FCC-ee Z-pole programme demonstrates why the Z and WW stages are essential for a robust Higgs interpretation. Source: FCC Feasibility Study Report Vol. 1 [1]; adapted from the SMEFT global-fit studies discussed therein.

1.8.4 Coupling modifiers and the κ-3 framework

The coupling-modifier or κ-framework provides a simple way to express projected Higgs precision. For a coupling g_i, one defines

$$\kappa_i = \frac{g_i}{g_i^{\mathrm{SM}}}, \tag{1.48}$$

or, for loop-induced modes, an effective modifier multiplying the Standard Model amplitude or rate. A production-times-decay rate can be written as

$$(\sigma \cdot \mathrm{BR})(i \to H \to f) = \sigma_i \, \frac{\Gamma_f}{\Gamma_H}. \tag{1.49}$$

In the κ-framework this becomes

$$(\sigma \cdot \mathrm{BR})(i \to H \to f) = \left(\sigma_i^{\mathrm{SM}} \kappa_i^2\right) \frac{\Gamma_f^{\mathrm{SM}} \kappa_f^2}{\Gamma_H^{\mathrm{SM}} \kappa_H^2}. \tag{1.50}$$

The corresponding signal strength is

$$\mu_i^f \equiv \frac{(\sigma \cdot \mathrm{BR})(i \to H \to f)}{(\sigma \cdot \mathrm{BR})_{\mathrm{SM}}(i \to H \to f)} = \frac{\kappa_i^2 \kappa_f^2}{\kappa_H^2}. \tag{1.51}$$

If only Standard-Model decay modes are allowed, the total-width modifier is approximately

$$\kappa_H^2 = \sum_j \kappa_j^2 \, \mathrm{BR}_j^{\mathrm{SM}}. \tag{1.52}$$

In the κ-3 framework used in the comparison plots, invisible and undetected or untagged Higgs decays are also allowed. One then defines

$$\bar{\kappa}_H^2 = \frac{\kappa_H^2}{1 - B_{\mathrm{inv}} - B_{\mathrm{und}}}, \qquad \Gamma_H = \bar{\kappa}_H^2 \, \Gamma_H^{\mathrm{SM}}. \tag{1.53}$$

Here B_{inv} is the invisible Higgs branching fraction and B_{und}, sometimes also written B_{unt}, denotes an undetected or untagged branching fraction.

Definition

The κ-3 framework. The κ-3 setup is a coupling-modifier fit in which Higgs coupling modifiers, an invisible branching fraction and an undetected/untagged branching fraction are fitted simultaneously. In the version shown here, the condition $\kappa_V \le 1$ for $V = W, Z$ is imposed to stabilise the fit. This condition is motivated by a broad class of models in which Higgs coupling to massive vector bosons is not enhanced above the Standard Model value, but it should still be understood as an assumption.

The following three figures show projected uncertainties in this framework. They separate the fitted quantities into fermion modifiers, vector and BSM modifiers, and loop-induced modifiers.

Figure 1.2 collects the fermionic Higgs coupling modifiers:

$$\kappa_b : \text{bottom Yukawa modifier, probed mainly by } H \to b\bar{b}, \tag{1.54}$$
$$\kappa_c : \text{charm Yukawa modifier, probed by } H \to c\bar{c}, \tag{1.55}$$
$$\kappa_\tau : \text{tau Yukawa modifier, probed by } H \to \tau^+\tau^-, \tag{1.56}$$
$$\kappa_\mu : \text{muon Yukawa modifier, probed by } H \to \mu^+\mu^-, \tag{1.57}$$
$$\kappa_t : \text{top Yukawa modifier, entering mainly through top-associated production, and loops.} \tag{1.58}$$

The vertical axis is the projected relative uncertainty in percent. The different colours correspond to different future-collider scenarios or combinations. The main qualitative point is that FCC-ee

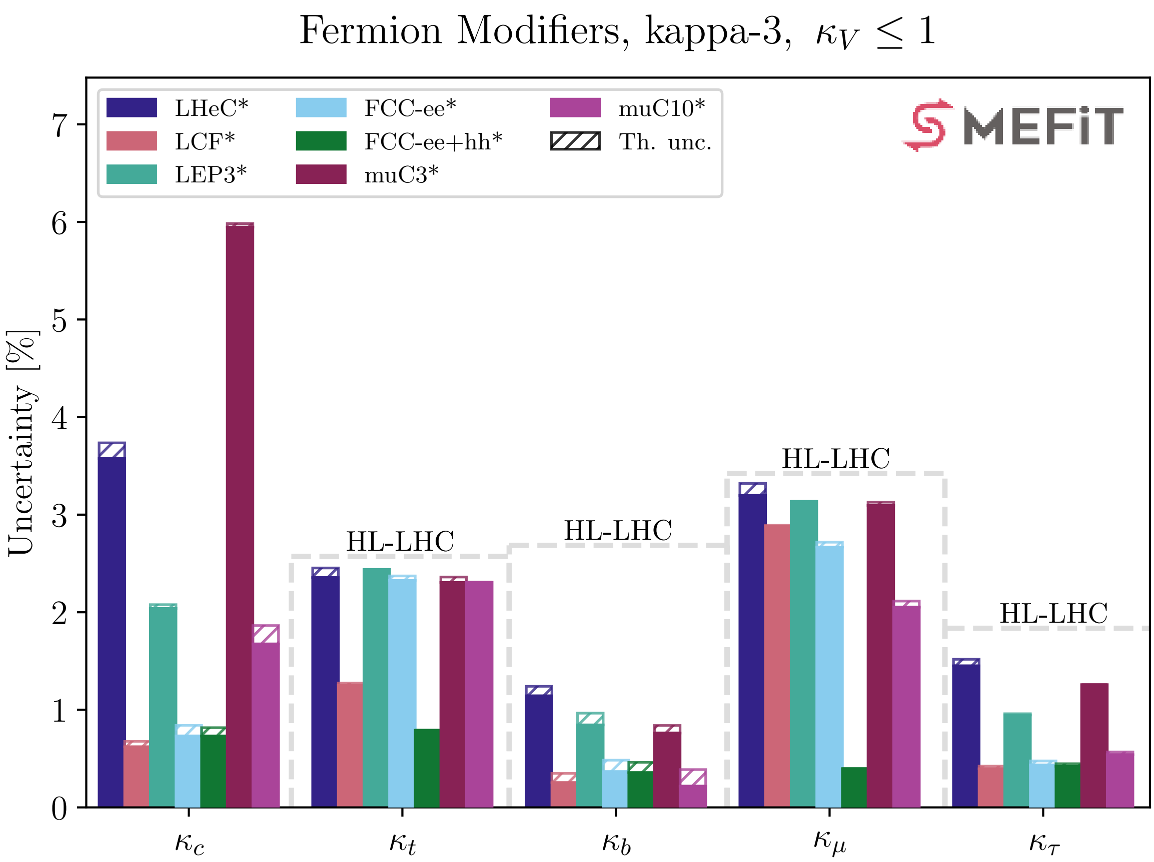

Figure 1.2: Projected uncertainties for fermion Higgs coupling modifiers in the κ-3 framework with a common HL-LHC baseline and the condition $\kappa_V \leq 1$. The fitted fermion modifiers are κ_c, κ_t, κ_b, κ_μ and κ_τ. Source: Ref. [5].

provides strong sub-percent or percent-level access to several Yukawa couplings through clean exclusive Higgs decays, while FCC-hh or other high-energy stages are important for κ_t and very rare modes.

Figure 1.3 focuses on the vector-boson and non-standard branching-fraction part of the fit:

$$\kappa_W : \text{modifier of the } HWW \text{ coupling,} \tag{1.59}$$

$$\kappa_Z : \text{modifier of the } HZZ \text{ coupling,} \tag{1.60}$$

$$B_{\text{inv}} : \text{invisible Higgs branching fraction,} \tag{1.61}$$

$$B_{\text{und}} : \text{undetected or untagged Higgs branching fraction.} \tag{1.62}$$

The most important FCC-ee ingredient here is the inclusive recoil measurement of $\sigma(ZH)$, which gives direct access to the absolute HZZ normalisation. Combined with WW-fusion information,

$$e^+e^- \to \nu\bar{\nu}H,$$

it provides a handle on Γ_H and separates κ_Z, κ_W and the total width. This is the reason why FCC-ee can perform a more model-independent Higgs coupling extraction than hadron-collider rate fits alone.

Figure 1.4 shows the loop-induced or effective Higgs modifiers:

$$\kappa_g : \text{effective } Hgg \text{ modifier,} \tag{1.63}$$

$$\kappa_\gamma : \text{effective } H\gamma\gamma \text{ modifier,} \tag{1.64}$$

$$\kappa_{Z\gamma} : \text{effective } HZ\gamma \text{ modifier.} \tag{1.65}$$

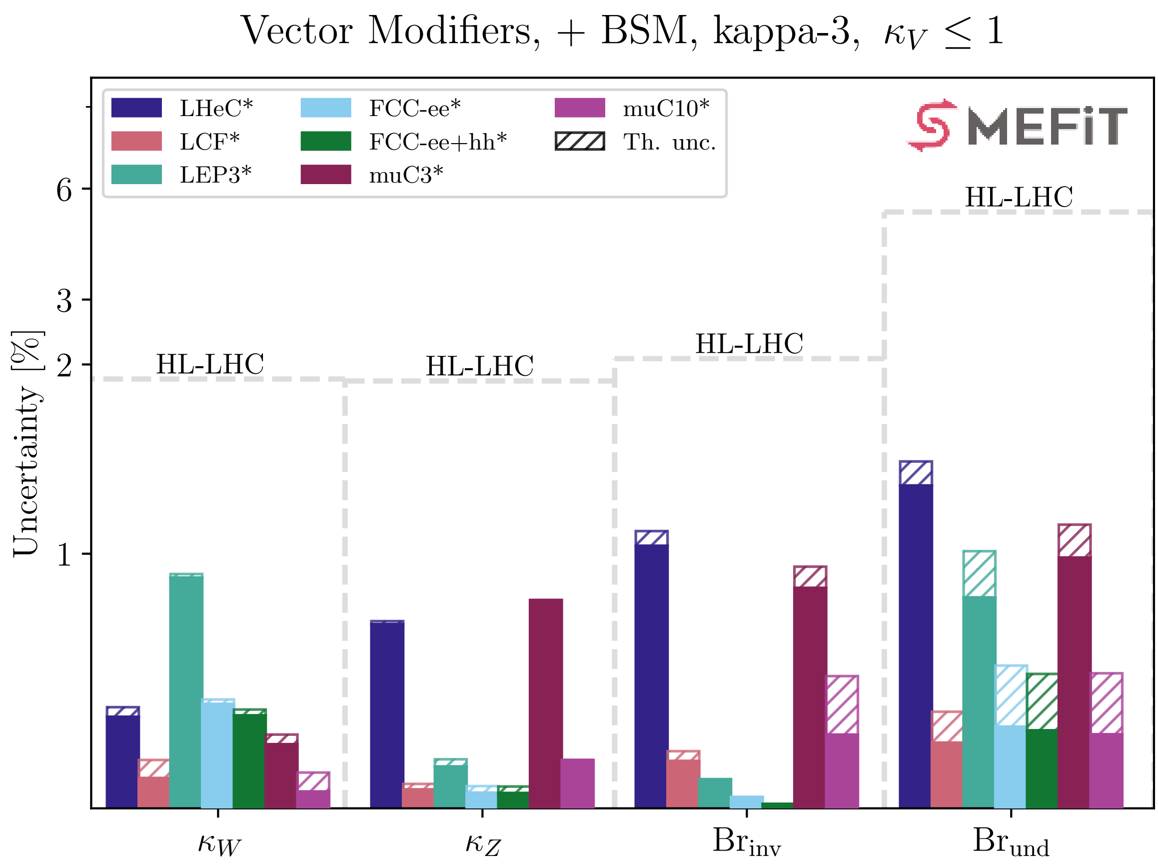

Figure 1.3: Projected uncertainties for vector-boson Higgs modifiers and additional BSM branching fractions in the κ-3 framework. The fitted quantities include κ_W, κ_Z, B_{inv} and B_{und}. Source: Ref. [5].

These are not simple tree-level Yukawa or gauge couplings. In the Standard Model they arise first through loops. For example, $H \to gg$ is dominated by heavy-quark loops, while $H \to \gamma\gamma$ receives important contributions from both W-boson and top-quark loops. As a result, these channels are sensitive not only to Standard-Model coupling modifications but also to possible new heavy coloured or electrically charged particles running in the loop. FCC-ee provides a clean normalisation and excellent flavour separation, while FCC-hh can strongly improve rare loop-induced modes through large Higgs statistics.

Key message

The κ-framework gives a useful experimental language for Higgs precision, while the SMEFT gives the gauge-invariant language needed to connect Higgs, electroweak, diboson and top observables. For the present talk, the important point is that the rare-top FCNC analysis is embedded in this broader precision programme: the same collider environment that gives absolute Higgs normalisation also enables clean top and rare-process measurements.

This completes the Higgs–electroweak bridge. We can now move to the top programme. The logic is analogous: top-threshold and above-threshold measurements are not isolated top measurements, but part of the same global precision programme. They constrain m_t, Γ_t, $t\bar{t}Z$ couplings, the top Yukawa interaction and SMEFT directions that are correlated with the Higgs and electroweak sectors.

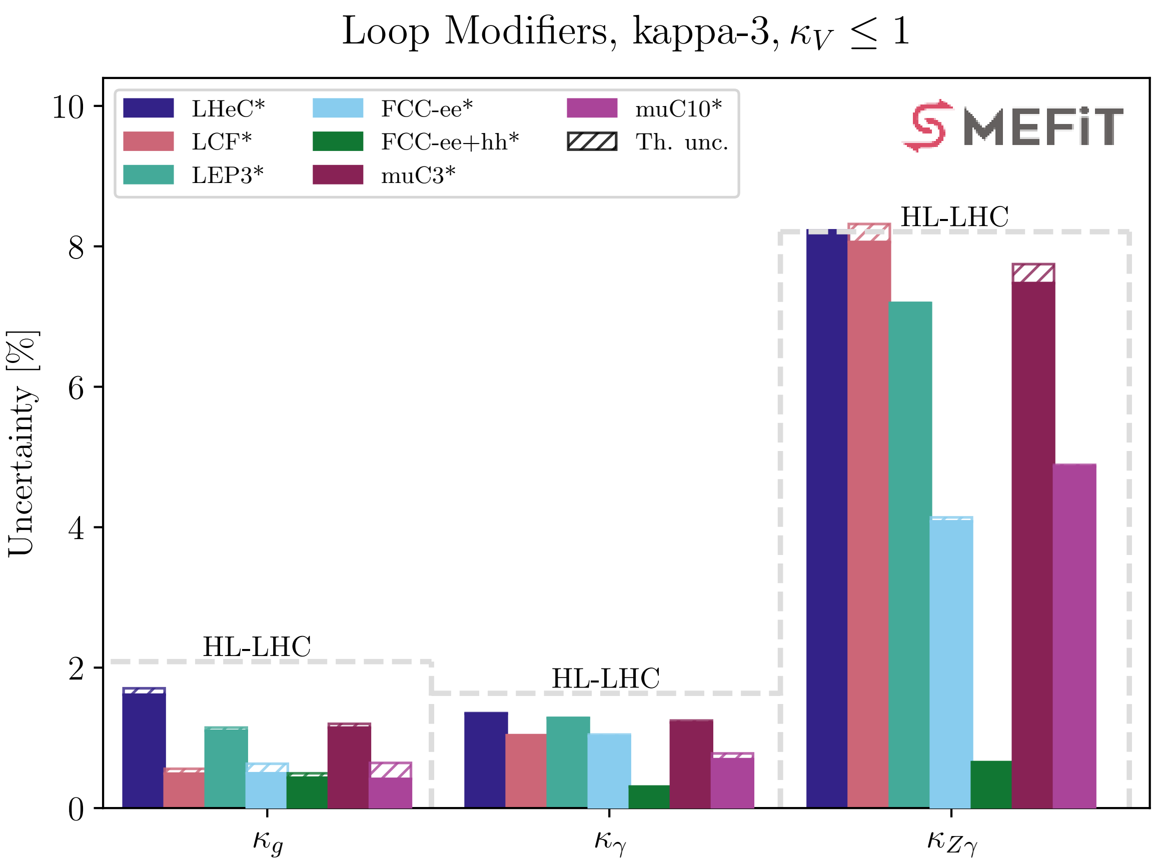

Figure 1.4: Projected uncertainties for loop-induced Higgs modifiers in the κ-3 framework. The fitted quantities are κ_g, κ_γ and $\kappa_{Z\gamma}$. Source: Ref. [5].

Table 1.3: Summary of the main coupling symbols introduced before the top-precision section.

Symbol	**Meaning**	**Main FCC-ee handle**
$\delta g^{Zf}_{L,R}$	Shift in left/right $Zf\bar{f}$ coupling	Z-pole line shape and asymmetries
δg^{H}_{ZZ}	Effective shift in HZZ interaction	Inclusive ZH recoil measurement
δg^{H}_{WW}	Effective shift in HWW interaction	WW-fusion, $H \to WW^*$
$\delta g^{H}_{\gamma\gamma}$	Effective $H\gamma\gamma$ shift	$H \to \gamma\gamma$, loop sensitivity
$\delta g^{H}_{Z\gamma}$	Effective $HZ\gamma$ shift	$H \to Z\gamma$, loop sensitivity
$\delta g_{1,Z}$	Anomalous WWZ coupling shift	$e^+e^- \to W^+W^-$ angular data
$\delta\kappa_\gamma$	Anomalous $WW\gamma$ dipole-like shift	W^+W^- production
λ_Z	Momentum-dependent WWZ coupling	Diboson angular distributions
κ_Z	HZZ coupling modifier	ZH recoil standard candle
κ_W	HWW coupling modifier	WW-fusion and $H \to WW^*$
$\kappa_b, \kappa_c, \kappa_\tau, \kappa_\mu$	Yukawa coupling modifiers	Exclusive Higgs decays with flavour/PID
κ_t	Top Yukawa modifier	Top/Higgs loops and FCC-hh input
$\kappa_g, \kappa_\gamma, \kappa_{Z\gamma}$	Loop-induced Higgs modifiers	Rare Higgs decays and global fits
B_{inv}	Invisible Higgs branching fraction	Recoil missing-rate analysis
B_{und} or B_{unt}	Undetected/untagged Higgs branching fraction	Inclusive recoil plus global fit

1.9 Top-quark precision at FCC-ee

The top threshold programme measures the final state

$$e^+e^- \to W^+bW^-\bar{b}, \tag{1.66}$$

with resonant and non-resonant contributions. The threshold line shape can be written schematically as

$$\sigma_{WbWb} = \sigma_{WbWb}(\sqrt{s}; m_t, \Gamma_t, \alpha_s, y_t). \tag{1.67}$$

The horizontal position of the line shape is sensitive to the top mass, the width controls the sharpness, α_s affects the QCD potential, and the top Yukawa coupling produces smaller but relevant effects through Higgs exchange. A threshold mass such as the potential-subtracted mass m_t^{PS} is used to avoid the pole-mass ambiguity.

Above threshold, the process

$$e^+e^- \to \gamma^*, Z^* \to t\bar{t} \tag{1.68}$$

probes the top electroweak vertex. A compact notation is

$$\mathcal{L}_{ttZ} = \frac{g}{2c_W}\bar{t}\gamma^\mu \left(g_V^t - g_A^t\gamma_5\right) tZ_\mu. \tag{1.69}$$

Angular distributions and forward–backward asymmetries are essential to separate chiral structures.

1.10 FCNC in the Standard Model and beyond

Flavour-changing neutral currents (FCNCs) such as $t \to q\gamma$, $t \to qZ$, $t \to qH$ and $t \to qg$ are absent at tree level in the SM. They appear only through loops and are strongly suppressed by the Glashow–Iliopoulos–Maiani mechanism. The expected branching ratios are tiny, often around 10^{-12} or below depending on the channel. Therefore any observable rate far above the SM expectation would strongly indicate BSM dynamics [7].

The talk focuses on $tq\gamma$ and tqZ because these interactions induce clean single-top production in e^+e^- collisions:

$$e^+e^- \to \gamma^*/Z^* \to t\bar{q},\ \bar{t}q, \qquad q = u, c. \tag{1.70}$$

The produced top decays through the SM mode

$$t \to Wb, \tag{1.71}$$

which leads to semileptonic and fully hadronic signatures.

1.11 Effective Lagrangian for top-FCNC interactions

The anomalous-coupling framework used in the slides follows the common Aguilar-Saavedra normalisation [8]. The interaction is

$$\mathcal{L}_{\mathrm{FCNC}}^{tqX} = \sum_{q=u,c}\Bigg[\frac{g_s}{2m_t}\bar{q}\lambda^a\sigma^{\mu\nu}(\zeta_{qt}^L P_L + \zeta_{qt}^R P_R)tG_{\mu\nu}^a - \frac{1}{\sqrt{2}}\bar{q}(\eta_{qt}^L P_L + \eta_{qt}^R P_R)tH \tag{1.72}$$

$$- \frac{g_W}{2c_W}\bar{q}\gamma^\mu(X_{qt}^L P_L + X_{qt}^R P_R)tZ_\mu + \frac{g_W}{4c_W m_Z}\bar{q}\sigma^{\mu\nu}(\kappa_{qt}^L P_L + \kappa_{qt}^R P_R)tZ_{\mu\nu} \tag{1.73}$$

$$+ \frac{e}{2m_t}\bar{q}\sigma^{\mu\nu}(\lambda_{qt}^L P_L + \lambda_{qt}^R P_R)tA_{\mu\nu}\Bigg] + \mathrm{h.c.} \tag{1.74}$$

Here $q = u, c$, g_s is the strong coupling, g_W the weak $SU(2)_L$ coupling, e the electromagnetic coupling, $c_W = \cos\theta_W$, λ^a are colour generators and $\sigma^{\mu\nu} = i[\gamma^\mu, \gamma^\nu]/2$. The field strengths are $G_{\mu\nu}^a$, $Z_{\mu\nu}$ and $A_{\mu\nu}$. The coefficients ζ, η, X, κ and λ parameterise, respectively, tqg, tqH, vector tqZ, dipole tqZ and dipole $tq\gamma$ interactions.

Caution

The benchmark assumption $\lambda^L = \lambda^R$ or $\kappa^L = \kappa^R$ is a practical signal-generation choice. It is not a model-independent statement. Different BSM models can generate strongly chiral patterns.

1.12 Translation between anomalous couplings and branching ratios

The branching ratio is defined as

$$\mathrm{Br}(t \to qX) = \frac{\Gamma(t \to qX)}{\Gamma_t^{\mathrm{SM}} + \sum_X \Gamma(t \to qX)} \simeq \frac{\Gamma(t \to qX)}{\Gamma_t^{\mathrm{SM}}}, \tag{1.75}$$

where the approximation holds for small FCNC widths. In the convention of Eq. (1.74), neglecting the light-quark mass, the photon-dipole partial width is commonly written as

$$\Gamma(t \to q\gamma) = \frac{\alpha}{4} m_t \left(|\lambda_{qt}^L|^2 + |\lambda_{qt}^R|^2 \right). \tag{1.76}$$

For the Z dipole, with $r_Z = m_Z^2/m_t^2$,

$$\Gamma(t \to qZ)_\kappa = \frac{\alpha}{32 s_W^2 c_W^2} \frac{m_t^3}{m_Z^2} (1 - r_Z)^2 (2 + r_Z) \left(|\kappa_{qt}^L|^2 + |\kappa_{qt}^R|^2 \right). \tag{1.77}$$

For the symmetric benchmark $\lambda^L = \lambda^R = \lambda$ and $\kappa^L = \kappa^R = \kappa$,

$$\mathrm{Br}(t \to q\gamma) \simeq \frac{\alpha m_t}{2\Gamma_t^{\mathrm{SM}}} |\lambda_{qt}|^2, \tag{1.78}$$

$$\mathrm{Br}(t \to qZ)_\kappa \simeq \frac{\alpha}{16 s_W^2 c_W^2} \frac{m_t^3}{m_Z^2 \Gamma_t^{\mathrm{SM}}} (1 - r_Z)^2 (2 + r_Z) |\kappa_{qt}|^2. \tag{1.79}$$

The numerical translation must use the same coupling normalisation as the UFO model used for event generation.

1.13 Signal processes at 240 and 365 GeV

The signal process is

$$e^+e^- \to t\bar{q} + \bar{t}q, \tag{1.80}$$

mediated by the anomalous $tq\gamma$ and tqZ couplings. At 240 GeV, the stage is optimised for Higgs studies but also provides clean single-top kinematics. At 365 GeV, there is more phase space and harder objects, but also genuine top backgrounds. The benchmark luminosities used in the slides are $5\,\mathrm{ab}^{-1}$ at 240 GeV and $1.5\,\mathrm{ab}^{-1}$ at 365 GeV.

1.14 Semileptonic and fully hadronic final states

The semileptonic topology is

$$e^+e^- \to tq \to Wbq \to \ell\nu bq, \tag{1.81}$$

with one isolated electron or muon, missing momentum from the neutrino, one b-tagged jet and one energetic light jet. It is clean but has a smaller branching fraction. The fully hadronic topology is

$$e^+e^- \to tq \to Wbq \to q\bar{q}'bq, \tag{1.82}$$

with four exclusive jets. It has a larger branching fraction but suffers from larger diboson backgrounds and combinatorics. A typical assignment variable is

$$\chi^2 = \frac{(m_{jj} - m_W)^2}{\sigma_W^2} + \frac{(m_{bjj} - m_t)^2}{\sigma_t^2}, \tag{1.83}$$

where the jet combination minimising χ^2 is chosen as the top candidate.

1.15 Backgrounds, jet clustering and flavour tagging

The dominant backgrounds are WW, ZZ, ZH, $e\gamma$ initiated processes, and at 365 GeV also $t\bar{t}$ and single-top-like final states. The analysis adopts the ee-k_T Durham algorithm in exclusive two-jet or four-jet modes. E-scheme recombination means four-momenta are added directly. The slides quote a flavour-tagging working point $\epsilon_b = 80\%$ and $\epsilon_c = 10\%$. In the FCNC selection, b tagging identifies the top decay, while light-jet rejection and charm/light separation control backgrounds.

Discriminating variables include reconstructed masses M_W and M_{top}, the b-jet momentum p_b, the light-jet momentum p_{light}, missing momentum, angular separations and event activity. If H_T is used, define it in the analysis note as the scalar sum of visible transverse momenta or the corresponding FCC-ee event-activity proxy:

$$H_T = \sum_i p_{T,i}. \tag{1.84}$$

The usual hadron-collider angular distance is

$$\Delta R = \sqrt{(\Delta\eta)^2 + (\Delta\phi)^2}, \tag{1.85}$$

although in e^+e^- analyses ordinary opening angles are often equally transparent.

1.16 Statistical analysis and CL$_s$ extraction

A generic binned likelihood for the combined analysis is

$$\mathcal{L}(\mu, \boldsymbol{\theta}) = \prod_{c,b} \text{Pois}\left(n_{cb} \,|\, \mu s_{cb}(\boldsymbol{\theta}) + b_{cb}(\boldsymbol{\theta})\right) \prod_k \pi_k(\theta_k), \tag{1.86}$$

where c labels channels, b labels histogram bins, n_{cb} are observed or Asimov counts, s_{cb} and b_{cb} are signal and background templates, μ is the signal-strength parameter, and θ_k are nuisance parameters. The CL$_s$ ratio is conventionally

$$CL_s = \frac{p_{s+b}}{1 - p_b}, \tag{1.87}$$

with the exclusion set at $CL_s = 0.05$ for a 95% CL upper limit. In projected studies the observed dataset is often an Asimov dataset, so the quoted limit is an expected sensitivity.

1.17 Interpretation of projected limits

The final tables quote limits on $\text{Br}(t \to c\gamma)$ and $\text{Br}(t \to cZ)$ rather than directly on λ and κ. This is useful for comparing with LHC results and with other future-collider projections. The lepton channel gives the best sensitivity in the present benchmark because the final state is cleaner and the backgrounds are more controllable. The hadronic channel still contributes because its branching fraction is larger and it probes a complementary topology. The results should be described as study-level projections, subject to the stated luminosities, detector assumptions, signal model and systematic-treatment assumptions.

Part II

Technical appendices

Appendix A

Coupling and notation dictionary

Symbol	Meaning
$\sqrt{s}$	Centre-of-mass energy of the e^+e^- collision.
m_Z, Γ_Z	Z-boson mass and total width.
m_W, Γ_W	W-boson mass and total width.
$\sin^2\theta_{\mathrm{eff}}^{\ell}$	Effective weak mixing angle measured in leptonic asymmetries.
R_b	Ratio $\Gamma_{b\bar{b}}/\Gamma_{\mathrm{had}}$.
N_ν	Effective number of light neutrino species inferred from invisible Z width.
$A_{\mathrm{FB}}^{0,f}$	Pole forward–backward asymmetry for fermion f.
P_L, P_R	Chiral projectors $(1 \mp \gamma_5)/2$.
g_L^f, g_R^f	Left- and right-handed Z couplings to fermion f.
g_V^f, g_A^f	Vector and axial-vector Z couplings.
$\delta g_{1,Z}$	Deviation in the WWZ triple-gauge coupling.
$\delta\kappa_\gamma$	Deviation in the $WW\gamma$ magnetic-dipole-like coupling.
λ_Z	Higher-derivative anomalous WWZ coupling.
κ_Z, κ_W	Higgs coupling modifiers for HZZ and HWW.
$\kappa_b, \kappa_c, \kappa_t$	Higgs Yukawa modifiers for bottom, charm and top.
$\kappa_g, \kappa_\gamma, \kappa_{Z\gamma}$	Effective loop-induced Higgs modifiers.
B_{inv}	Invisible Higgs branching ratio.
B_{und} or B_{unt}	Undetected/untagged Higgs branching ratio.
Γ_H	Total Higgs width.
m_t^{PS}	Potential-subtracted top mass used for threshold fits.
ζ_{qt}	Chromomagnetic tqg FCNC coefficient.
η_{qt}	Scalar tqH FCNC coefficient.
X_{qt}	Vector tqZ FCNC coefficient.
κ_{qt}	Dipole tqZ FCNC coefficient.
λ_{qt}	Dipole $tq\gamma$ FCNC coefficient.
ϵ_b, ϵ_c	b-tagging efficiency and charm-tagging/mistag working-point number as used in the analysis.
CL_s	Modified frequentist confidence-level ratio used for expected upper limits.

Appendix B

Electroweak formula sheet

$$\sigma^0_{\text{had}} = \frac{12\pi}{m_Z^2}\frac{\Gamma_e\Gamma_{\text{had}}}{\Gamma_Z^2}, \qquad R_\ell = \frac{\Gamma_{\text{had}}}{\Gamma_{\ell\ell}}, \qquad R_b = \frac{\Gamma_{b\bar{b}}}{\Gamma_{\text{had}}}, \tag{B.1}$$

$$A_f = \frac{(g_L^f)^2 - (g_R^f)^2}{(g_L^f)^2 + (g_R^f)^2}, \qquad A^{0,f}_{\text{FB}} = \frac{3}{4}A_e A_f, \qquad N_\nu = \frac{\Gamma_{\text{inv}}}{\Gamma_\nu^{\text{SM}}}. \tag{B.2}$$

A full FCC electroweak fit also includes QED radiator functions, beam-energy calibration, luminosity theory and correlations among pseudo-observables.

Appendix C

Higgs recoil and coupling-extraction formula sheet

$$m^2_{\mathrm{recoil}} = s + m_Z^2 - 2\sqrt{s}E_Z, \tag{C.1}$$

$$\sigma(ZH) \propto \kappa_Z^2, \tag{C.2}$$

$$\sigma(ZH)\mathrm{Br}(H \to X) \propto \frac{\kappa_Z^2 \kappa_X^2}{\Gamma_H}, \tag{C.3}$$

$$\sigma(\nu\bar{\nu}H)\mathrm{Br}(H \to X) \propto \frac{\kappa_W^2 \kappa_X^2}{\Gamma_H}, \tag{C.4}$$

$$\mu_i^f = \frac{\kappa_i^2 \kappa_f^2}{\kappa_H^2}, \tag{C.5}$$

$$\bar{\kappa}_H^2 = \frac{\kappa_H^2}{1 - B_{\mathrm{inv}} - B_{\mathrm{und}}}. \tag{C.6}$$

Appendix D

SMEFT operator map

Operator	Main effect
$\mathcal{O}_{HWB}$	Shifts electroweak mixing and correlates EWPOs with Higgs-gauge couplings.
$\mathcal{O}_{HD}$	Affects custodial-sensitive electroweak observables and Higgs-gauge interactions.
$\mathcal{O}_{H\ell}^{(1)}$, $\mathcal{O}_{H\ell}^{(3)}$	Shift lepton electroweak currents, including Zee and $We\nu$.
$\mathcal{O}_{He}$	Shifts right-handed electron coupling to the Z.
$\mathcal{O}_{HW}$, $\mathcal{O}_{HB}$	Modify Higgs-gauge and diboson interactions.
$\mathcal{O}_{W}$	Produces momentum-dependent triple-gauge-coupling deviations.
Top dipoles and currents	Affect top EW couplings and loop-induced Higgs/top correlations.

Appendix E

Top-FCNC branching-ratio formula sheet

For the convention used in the slides,

$$\Gamma(t \to q\gamma) = \frac{\alpha}{4} m_t (|\lambda_{qt}^L|^2 + |\lambda_{qt}^R|^2), \tag{E.1}$$

$$\Gamma(t \to qZ)_\kappa = \frac{\alpha}{32 s_W^2 c_W^2} \frac{m_t^3}{m_Z^2} (1 - r_Z)^2 (2 + r_Z)(|\kappa_{qt}^L|^2 + |\kappa_{qt}^R|^2), \tag{E.2}$$

$$\mathrm{Br}(t \to qX) \simeq \Gamma(t \to qX)/\Gamma_t^{\mathrm{SM}}, \qquad r_Z = m_Z^2/m_t^2. \tag{E.3}$$

Caution

These expressions must not be combined with a differently normalised FCNC Lagrangian. If another UFO model is used, the conversion between coupling limits and branching ratios must be rederived or checked against the model documentation.

Appendix F

Analysis checklist

1. Generate FCNC signal with one anomalous coupling switched on at a time.
2. Simulate detector response in the official FCC chain or a documented Delphes/IDEA approximation.
3. Reconstruct exclusive two-jet and four-jet topologies with the selected ee-Durham algorithm.
4. Apply lepton, jet, angular and flavour-tagging selections.
5. Build signal and background templates for discriminating variables.
6. Construct channel-wise likelihoods and combine channels/energies.
7. Translate signal-strength limits into branching-ratio limits using the same Lagrangian normalisation.
8. Repeat with systematic uncertainties and possibly multivariate discriminants for a final public analysis.

Appendix G

Extended formula compendium

This appendix collects compact formulae that are useful during Q&A. They are intentionally redundant with the main text, because they provide a quick technical lookup while presenting.

G.1 Kinematics and event reconstruction

$$
\begin{aligned}
s &= (p_{e^+} + p_{e^-})^2, & E_{\mathrm{beam}} &= \sqrt{s}/2, && \text{(G.1)}\\
p^\mu_{\mathrm{miss}} &= p^\mu_{e^+} + p^\mu_{e^-} - \sum_i p^\mu_i, & E_{\mathrm{miss}} &= p^0_{\mathrm{miss}}, && \text{(G.2)}\\
m^2_{ij} &= (p_i + p_j)^2, & m^2_{bjj} &= (p_b + p_{j_1} + p_{j_2})^2, && \text{(G.3)}\\
H_T &= \sum_i p_{T,i}, & \Delta R_{ij} &= \sqrt{(\eta_i - \eta_j)^2 + (\phi_i - \phi_j)^2}, && \text{(G.4)}\\
\cos\theta_{ij} &= \frac{\vec{p}_i \cdot \vec{p}_j}{|\vec{p}_i||\vec{p}_j|}, & \chi^2_W &= \frac{(m_{jj} - m_W)^2}{\sigma^2_W}, && \text{(G.5)}\\
\chi^2_t &= \frac{(m_{bjj} - m_t)^2}{\sigma^2_t}, & \chi^2_{\mathrm{tot}} &= \chi^2_W + \chi^2_t. && \text{(G.6)}
\end{aligned}
$$

G.2 Electroweak couplings

$$
\begin{aligned}
Q_e &= -1, & T_3^{e_L} &= -\frac{1}{2}, \quad T_3^{\nu_L} = +\frac{1}{2}, && \text{(G.7)}\\
g^f_L &= T^f_3 - Q_f s^2_{\mathrm{eff}}, & g^f_R &= -Q_f s^2_{\mathrm{eff}}, && \text{(G.8)}\\
g^f_V &= g^f_L + g^f_R, & g^f_A &= g^f_L - g^f_R, && \text{(G.9)}\\
\Gamma_f &= N^f_c \frac{G_F m^3_Z}{6\sqrt{2}\pi}\left[(g^f_V)^2 + (g^f_A)^2\right](1 + \delta_f), &&&& \text{(G.10)}\\
A_f &= \frac{2 g^f_V g^f_A}{(g^f_V)^2 + (g^f_A)^2}, & A^{0,f}_{\mathrm{FB}} &= \frac{3}{4} A_e A_f, && \text{(G.11)}\\
R_b &= \Gamma_b/\Gamma_{\mathrm{had}}, & R_c &= \Gamma_c/\Gamma_{\mathrm{had}}, && \text{(G.12)}\\
\Gamma_Z &= \sum_f \Gamma_f + \Gamma_{\mathrm{inv}}, & \Gamma_{\mathrm{inv}} &= N_\nu \Gamma^{\mathrm{SM}}_\nu. && \text{(G.13)}
\end{aligned}
$$

G.3 Higgs rates

$$\sigma_{ZH} = \kappa_Z^2 \sigma_{ZH}^{\rm SM}, \qquad \Gamma_X = \kappa_X^2 \Gamma_X^{\rm SM}, \tag{G.14}$$

$$\mathrm{Br}_X = \Gamma_X/\Gamma_H, \qquad \mu_i^f = \frac{\sigma_i \mathrm{Br}_f}{(\sigma_i \mathrm{Br}_f)_{\rm SM}}, \tag{G.15}$$

$$\mu_i^f = \frac{\kappa_i^2 \kappa_f^2}{\kappa_H^2}, \qquad \kappa_H^2 = \sum_j \kappa_j^2 \mathrm{Br}_j^{\rm SM}, \tag{G.16}$$

$$\bar{\kappa}_H^2 = \frac{\kappa_H^2}{1 - B_{\rm inv} - B_{\rm und}}, \qquad \Gamma_H = \bar{\kappa}_H^2 \Gamma_H^{\rm SM}, \tag{G.17}$$

$$\sigma(ZH)\mathrm{Br}_{b\bar{b}} \propto \frac{\kappa_Z^2 \kappa_b^2}{\Gamma_H}, \qquad \sigma(ZH)\mathrm{Br}_{ZZ^*} \propto \frac{\kappa_Z^4}{\Gamma_H}, \tag{G.18}$$

$$\sigma(\nu\bar{\nu}H)\mathrm{Br}_X \propto \frac{\kappa_W^2 \kappa_X^2}{\Gamma_H}, \qquad m_{\rm recoil}^2 = s + m_Z^2 - 2\sqrt{s}E_Z. \tag{G.19}$$

G.4 SMEFT expansion and fit structure

$$\mathcal{L}_{\rm SMEFT} = \mathcal{L}_{\rm SM} + \sum_i \frac{C_i}{\Lambda^2}\mathcal{O}_i + \cdots, \tag{G.20}$$

$$\mathcal{A} = \mathcal{A}_{\rm SM} + \sum_i \frac{C_i}{\Lambda^2}\mathcal{A}_i, \tag{G.21}$$

$$\sigma = \sigma_{\rm SM} + \sum_i \frac{C_i}{\Lambda^2}\sigma_i^{\rm int} + \sum_{ij} \frac{C_i C_j}{\Lambda^4}\sigma_{ij}^{\rm quad}, \tag{G.22}$$

$$\chi^2(\vec{C}) = (\vec{O}_{\rm exp} - \vec{O}_{\rm th}(\vec{C}))^T V^{-1} (\vec{O}_{\rm exp} - \vec{O}_{\rm th}(\vec{C})), \tag{G.23}$$

$$\delta_{\rm tot}^2 = \delta_{\rm stat}^2 + \delta_{\rm syst}^2 + \delta_{\rm th}^2 + \delta_{\rm param}^2. \tag{G.24}$$

G.5 Top FCNC partial widths and yields

$$N_S = \sigma_S \mathcal{L} \epsilon_S, \qquad N_B = \sigma_B \mathcal{L} \epsilon_B, \tag{G.25}$$

$$Z_A = \sqrt{2\left[(S+B)\ln\left(1 + \frac{S}{B}\right) - S\right]}, \qquad Z_{S/\sqrt{B}} \simeq S/\sqrt{B}, \tag{G.26}$$

$$\Gamma(t \to q\gamma) = \frac{\alpha}{4} m_t (|\lambda_L|^2 + |\lambda_R|^2), \tag{G.27}$$

$$\Gamma(t \to qZ)_\kappa = \frac{\alpha}{32 s_W^2 c_W^2} \frac{m_t^3}{m_Z^2}(1 - r_Z)^2 (2 + r_Z)(|\kappa_L|^2 + |\kappa_R|^2), \tag{G.28}$$

$$\mathrm{Br}(t \to qX) \simeq \Gamma(t \to qX)/\Gamma_t^{\rm SM}, \qquad r_Z = m_Z^2/m_t^2, \tag{G.29}$$

$$\mathcal{L}(\mu, \theta) = \prod_{c,b} \mathrm{Pois}(n_{cb} | \mu s_{cb}(\theta) + b_{cb}(\theta)) \prod_k \pi_k(\theta_k), \tag{G.30}$$

$$q_\mu = -2 \ln \frac{\mathcal{L}(\mu, \hat{\hat{\theta}}_\mu)}{\mathcal{L}(\hat{\mu}, \hat{\theta})}, \qquad CL_s = \frac{p_{s+b}}{1 - p_b}. \tag{G.31}$$

Part III

Glossary and references

Appendix H

Glossary

Term	Explanation
FCC	Future Circular Collider.
FCC-ee	Electron–positron stage of the FCC integrated programme.
FCC-hh	Proton–proton stage of the FCC integrated programme.
HL-LHC	High-Luminosity Large Hadron Collider.
Tera-Z	FCC-ee Z-pole programme with about 10^{12} Z bosons.
EWPO	Electroweak precision observable.
SMEFT	Standard Model Effective Field Theory.
EFT	Effective Field Theory.
BSM	Beyond the Standard Model.
FCNC	Flavour-changing neutral current.
GIM	Glashow–Iliopoulos–Maiani suppression mechanism.
Higgsstrahlung	Associated production $e^+e^- \to ZH$.
Recoil mass	Mass inferred from the system recoiling against the reconstructed Z boson.
VBF	Vector-boson fusion.
WW threshold	Energy region near $e^+e^- \to W^+W^-$ threshold.
aTGC	Anomalous triple-gauge coupling.
IDEA	Innovative Detector for Electron-positron Accelerators.
EDM4HEP	Event Data Model for High-Energy Physics.
FCCSW	FCC software framework.
FCCAnalyses	FCC analysis framework for processing EDM4HEP samples.
UFO	Universal FeynRules Output model format.
CL_s	Modified frequentist method for exclusion limits.
Asimov dataset	Representative dataset equal to the expectation, used for expected sensitivities.

Bibliography

[1] FCC Collaboration, *Future Circular Collider Feasibility Study Report Volume 1: Physics, Experiments, Detectors*, Eur. Phys. J. C 85 (2025) 1468, arXiv:2505.00272.

[2] FCC Collaboration, *FCC Physics Opportunities: Future Circular Collider Conceptual Design Report Volume 1*, Eur. Phys. J. C 79 (2019) 474.

[3] A. Blondel et al., *The FCC integrated programme: a physics manifesto*, arXiv:2504.02634.

[4] ECFA Higgs, Electroweak and Top Factory Study, CERN Yellow Report Monograph 5/2025, arXiv:2506.15390.

[5] T. Armadillo et al., *New Physics Reach through Precision at Future Colliders: a Multi-Pronged Approach*, arXiv:2604.16596.

[6] M. M. Defranchis, J. de Blas, A. Mehta, M. Selvaggi and M. Vos, *A detailed study on the prospects for a $t\bar{t}$ threshold scan in e^+e^- collisions*, JHEP 11 (2025) 020, arXiv:2503.18713.

[7] J. A. Aguilar-Saavedra, *Top flavour-changing neutral interactions: Theoretical expectations and experimental detection*, Acta Phys. Polon. B35 (2004) 2695, hep-ph/0409342.

[8] J. A. Aguilar-Saavedra, *A minimal set of top anomalous couplings*, Nucl. Phys. B812 (2009) 181, arXiv:0811.3842.

[9] P. Azzi, H. Khanpour, M. Mohammadi Najafabadi, E. Perez and S. Tizchang, *Top quark FCNC anomalous couplings at the future collider FCC-ee*, FCC Physics and Experiments note, CERN repository record avxy7-mtz86.

[10] M. Cobal et al., *Bottom quark forward-backward asymmetry at the future electron-positron collider FCC-ee*, FCC Physics and Experiments note, CERN repository record g97j3-q0w73.

[11] IDEA detector concept for FCC-ee, arXiv:2502.21223.

[12] FCCAnalyses documentation, https://hep-fcc.github.io/FCCAnalyses/.

[13] CMS Higgs Combine Tool, https://github.com/cms-analysis/HiggsAnalysis-CombinedLimit.

[14] ATLAS Collaboration, HL-LHC prospects for top FCNC, ATL-PHYS-PUB-2019-001.

[15] CMS Collaboration, HL-LHC prospects for top FCNC, CMS-CR-2018-094.